Ann. Geophys., 30, 1271–1283, 2012
www.ann-geophys.net/30/1271/2012/
doi:10.5194/angeo-30-1271-2012

Annales Geophysicae

Low-frequency magnetic field fluctuations in Earth's plasma environment observed by THEMIS

L. Guicking, K.-H. Glassmeier, H.-U. Auster, Y. Narita, and G. Kleindienst

Institut für Geophysik und extraterrestrische Physik, Technische Universität Braunschweig, Mendelssohnstrasse 3, 38106 Braunschweig, Germany

Correspondence to: L. Guicking (l.guicking@tu-bs.de)

Received: 9 February 2012 – Revised: 18 June 2012 – Accepted: 19 July 2012 – Published: 27 August 2012

Abstract. Low-frequency magnetic wave activity in Earth's plasma environment was determined based on a statistical analysis of THEMIS magnetic field data. We observe that the spatial distribution of low-frequency magnetic field fluctuations reveals highest values in the magnetosheath, but the observations differ qualitatively from observations at Venus presented in a previous study since significant wave activity at Earth is also observed in the nightside magnetosheath. Outside the magnetosheath the low-frequency wave activity level is generally very low. By means of an analytical streamline model for the magnetosheath plasma flow, we are able to investigate the spatial and temporal evolution of wave intensity along particular streamlines in order to characterise possible wave generation mechanisms. We observe a decay of wave intensity along the streamlines, but contrary to the situation at Venus, we obtain good qualitative agreement with the theoretical concept of freely evolving/decaying turbulence. Differences between the dawn region and the dusk region can be observed only further away from the magnetopause. We conclude that wave generation mechanisms may be primarily attributed to processes at or in the vicinity of the bow shock. The difference with the observations of the Venusian magnetosheath we interpret to be the result of the different types of solar wind interaction processes since the Earth possesses a global magnetic field while Venus does not, and therefore the observed magnetic wave activities may be caused by diverse magnetic field controlled characteristics of wave generation processes.

Keywords. Magnetospheric physics (Magnetosheath; MHD waves and instabilities) – Space plasma physics (Turbulence)

1 Introduction

In Earth's solar wind interaction region, a variety of low-frequency magnetic field fluctuations is observed. The term "low-frequency" is used here in the same sense as in Guicking et al. (2010), Espley et al. (2004), and Schwartz et al. (1996): frequencies below or at the proton gyrofrequency. Great efforts have been undertaken to characterise and identify different wave modes (cf. e.g. the review of Schwartz et al., 1996). For instance, Narita and Glassmeier (2005) derived dispersion relations of low-frequency waves upstream and downstream of the terrestrial bow shock in order to improve the understanding of wave transmission, mode conversion, and wave excitation in the vicinity of the bow shock. Furthermore, Denton et al. (1998) determined transport ratios in order to identify wave modes and Anderson et al. (1994) focused on magnetic spectral signatures with respect to the occurrence of mirror modes and cyclotron waves. With the four satellites of the CLUSTER mission (e.g. Escoubet et al., 2001), one has the additional possibility to determine wave propagation directions and wave vectors, respectively. The studies of, e.g. Narita and Glassmeier (2006) and Schäfer et al. (2005), focused on this topic. Du et al. (2010) studied magnetosheath magnetic field variations based on DOUBLE STAR TC-1 and CLUSTER observations with periods from 4 s to 240 s (corresponding to a frequency range from 4 mHz to 250 mHz) for a data set of the year 2004. They found a dependency on the fluctuation characteristics from the angle of the interplanetary magnetic field orientation with respect to the bow shock normal, particularly, more intense fluctuations at smaller angles.

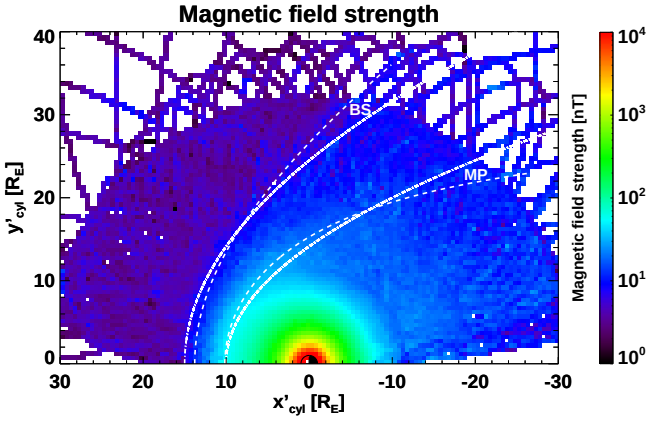

Fig. 1. Spatial distribution of the magnetic field strength (colour-coded) in Earth's plasma environment measured by THEMIS during the period March 2007 to February 2010. Data are binned and presented in cylindrical coordinates. The dashed and dashed-dotted lines represent bow shock (BS) and magnetopause (MP) models derived from spacecraft measurements and a theoretical model.

NASA's current satellite mission to study geomagnetic substorms, THEMIS (Angelopoulos, 2008; Sibeck and Angelopoulos, 2008), operates in the near Earth plasma environment and provides simultaneous measurements of five spacecraft. The satellites cover large areas of Earth's solar wind interaction region (Frey et al., 2008). Therefore, the THEMIS data are very suitable for a statistical investigation and the magnetic field data set provides a unique possibility to study globally magnetic field fluctuations in Earth's plasma environment under solar minimum conditions. In particular, primarily two satellites (THEMIS-B and THEMIS-C) expand into the magnetosheath and cross the bow shock, respectively, so that they even stay temporarily in the upstream solar wind. In July 2009 the ARTEMIS mission (Angelopoulos, 2011) has started and the THEMIS-B and the THEMIS-C spacecraft were navigated into transfer orbits to the Moon. This flight manoeuvre is associated with a spatial coverage of plasma regions still further away from Earth.

Liu et al. (2009) studied statistically the spatial distribution of Pc4 and Pc5 ULF pulsations in the inner magnetosphere on the basis of THEMIS electric and magnetic field observations. They conclude that the field line resonance and the Kelvin-Helmholtz instability may be important sources of the ULF waves and that the results are important with regard to the characterisation of Pc4 and Pc5 waves and the transport of energetic particles. Liu et al. (2010) extended the investigation of ULF wave intensity to a larger data set and studied the dependency on solar wind parameters.

The aim of this study is to provide a global overview of the low-frequency magnetic field fluctuation pattern in Earth's plasma environment based on a statistical analysis of the comprehensive THEMIS magnetic field data set. The results are compared to a study based on a similar data analysis procedure at Venus by Guicking et al. (2010) and thus it allows us to compare the low-frequency characteristics of two types of interaction processes of the solar wind with planetary obstacles: with Earth where its magnetic field characterises the interaction process and with Venus where no intrinsic magnetic field is believed to exist and as a consequence its dense atmosphere interacts directly with the solar wind.

2 Data analysis and results

We use in this study THEMIS magnetometer data from March 2007 to February 2010 which were recorded during 5450 days in total by the five spacecraft. The temporal resolution Δt of the data is 3 s, which allows us to resolve frequencies up to a maximum of 167 mHz (Nyquist frequency $f_{\mathrm{Nyq}} = (2\Delta t)^{-1}$). The frequency range below 167 mHz includes the low-frequency range in many regions of the solar wind interaction region of Earth, in particular the magnetosheath, as the proton gyrofrequency $\omega_{\mathrm{p}} = qB/m$ (q: electric charge, B: magnetic field strength, m: mass of protons) of 167 mHz corresponds to a magnetic field strength of ∼11 nT (cf. Fig. 1).

The data are given initially in geocentric solar ecliptic (GSE) coordinates in which the x-axis points from Earth towards the sun, the z-axis is perpendicular to the ecliptic plane pointing northward and the y-axis completes the right-handed coordinate system pointing into the opposite direction of the planetary motion (e.g. Song and Russell, 1999). The GSE coordinate system is useful for e.g. bow shock and magnetosheath phenomena, so for problems in which the orientation of Earth's dipole axis is less important than for problems in which the orientation plays an important role as e.g. magnetospheric phenomena (Song and Russell, 1999). The data were first transferred into the aberrated geocentric solar ecliptic (AGSE) coordinate system (x',y',z'). The aberration is realised by a constant 5° rotation of the coordinate system around the z-axis due to Earth's orbital velocity with respect to the solar wind flow velocity. The x'-axis has a better alignment with the incident solar wind flow direction and due to that it reduces on average the systematic error caused by Earth's orbital motion (cf. with e.g. Plaschke et al., 2009, who defined the same rotation of the GSE related geocentric solar magnetospheric coordinate system).

In Fig. 1 the spatial distribution of the magnetic field strength observed by the five THEMIS satellites for the analysed data set is displayed. The coordinate system in Fig. 1 is a cylindrical coordinate system which arises from the AGSE coordinate system by averaging the magnetic field strength around the x'-axis. The three directions of the magnetic field measurements are hence projected to a two-dimensional figure where $x'_{\mathrm{cyl}} = x'$ represents the apparent solar wind direction and $y'_{\mathrm{cyl}} = \sqrt{y'^2 + z'^2}$ the distance from the x'_{cyl}-axis. The magnetic field data are binned in the figure and the bin

size is $0.5\,R_E \times 0.5\,R_E$ (R_E:radius of Earth). The mean magnetic field strength of each bin is colour-coded.

Models of the bow shock (BS) and the magnetopause (MP) are also plotted for orientation. The dashed lines represent a bow shock model from Slavin and Holzer (1981) and a magnetopause model from Shue et al. (1997). Earth's bow shock is modelled by the equation (polar form)

$$r = \frac{L}{1+\epsilon\cos\theta}, \tag{1}$$

where L is the semi-latus rectum and ϵ the eccentricity. We used $L = 23.3\,R_E$ and $\epsilon = 1.16$. These values are mean parameters obtained from model fits which were performed on the basis of the bow shock crossings of the missions EXPLORER 28 (IMP 3), EXPLORER 34 (IMP 4), HEOS 1, PROGNOZ 1 and PROGNOZ 2. The hyperbola (Eq. 1) is shifted in the model by $x_0 = 3\,R_E$ in positive direction along the x-axis, which means that the bow shock stand-off distance writes as

$$R_s = x_0 + \frac{L}{1+\epsilon}. \tag{2}$$

Slavin and Holzer (1981) restrict their model to $-10\,R_E$ in the anti-sunward direction. Furthermore, they conclude that the bow shock shape and position vary only minimally during the solar cycle for the data set (standard deviations σ of the parameters L and ϵ: $\sigma_L = 0.3$, and $\sigma_\epsilon = 0.05$), and thus we consider the bow shock model and the chosen values for L and ϵ suitable to show the approximate position of transition between the solar wind and the magnetosheath.

The magnetopause is modelled by the equation (polar form)

$$r = r_0\left(\frac{2}{1+\cos\theta}\right)^{\alpha}, \tag{3}$$

where r_0 is the stand-off distance and α is the level of tail flaring. We used here $r_0 = 10.15\,R_E$ and $\alpha = 0.59$ (for that we used implicit $B_z = 0$ and a dynamic pressure of $D_p = 1.915$ nPa). These fit parameters were derived on the basis of the measurements of the ISEE 1, ISSE 2, AMPTE/IRM and EXPLORER 50 (IMP 8) missions. The magnetopause model was plotted by Shue et al. (1997) up to $-40\,R_E$ in the anti-sunward direction. As the shape and position are controlled by the solar activity, we have chosen a dynamic pressure which is typical for solar minimum conditions according to low solar activity during the period of selected measurements. Thus, we consider the magnetopause model with the chosen and derived values for B_z, D_p, r_0, and α suitable to show the approximate position of transition between the magnetosheath and the magnetosphere.

The dashed-dotted lines represent models of the bow shock and the magnetopause derived from parabolic coordinates, which are presented in more detail in Sect. 3 and are accompanied by a magnetosheath streamline model.

In Fig. 1 the dipole-like character of Earth's magnetic field with a magnetic field strength of more than 10 000 nT close to the planet is clearly visible. Furthermore, the compression of the magnetic field on the dayside due to the planetary obstacle accompanied by the deflection of the solar wind around the magnetopause, as well as the formation of the tail structure on the nightside characterised by an enhanced magnetic field strength (relative to the solar wind magnetic field strength upstream of the bow shock), can be observed. Data gaps in the upstream solar wind region and the tail region close to the x'_{cyl}-axis are due to gaps in the data set itself and a lower spatial coverage of measurements in these regions as well as the data selection process for the spectral analysis described later in this section.

For our statistical study with the focus on the low-frequency wave activity, we picked out intervals with a length of 102 s from the data set. Each following interval is shifted 3 s forward. Data gaps greater than 4.5 s occurring occasionally in the data set have not been considered, meaning that intervals containing these gaps are excluded from the analysis. The length of the intervals is a compromise between the temporal and spatial resolution as well as the presence of data gaps. Due to the different orbit geometries of the satellites, the spatial coverage is inhomogeneous, but a sufficient coverage is overall still achieved. We note that we did not consider data within a distance of $6.5\,R_E$ around Earth, because a range change of the instrument leads to significant artificial wave activity (the 3 pT resolution of the magnetic field data becomes more coarse during high magnetic field strengths; Auster et al., 2008). The frequency range considered in this study is 30 to 167 mHz, as our focus is on the low-frequency range. We note that it may be also worthwhile to investigate frequencies below this frequency range in more detail, but increasing the frequency resolution is at the expense of the spatial resolution and thus it is always an issue which has to be balanced.

The further wave activity calculation described in this paragraph was done in the same way as it was performed by Guicking et al. (2010) for magnetic field data of Venus' solar wind interaction region on the basis of the analysis methods of Song and Russell (1999), with the goal to determine a mean wave intensity value for each interval ensuring a comparison of the results for Earth and Venus. The data were transformed into a mean field aligned (MFA) coordinate system in which one axis points into the direction of the mean magnetic field. The data are then Fourier transformed into frequencies, and with the Fourier transform $\boldsymbol{B}(\omega)$ the power spectral density matrix

$$P_{ij} = \langle B_i(\omega)\,B_j^*(\omega)\rangle \tag{4}$$

was calculated (i, $j = 1, 2, 3$ are the three components of the magnetic field; the asterisk denotes the complex-conjugate). Finally, the minimum variance analysis was applied to the data, yielding the three eigenvectors and eigenvalues (λ_1,λ_2,λ_3) for the maximum, intermediate, and minimum

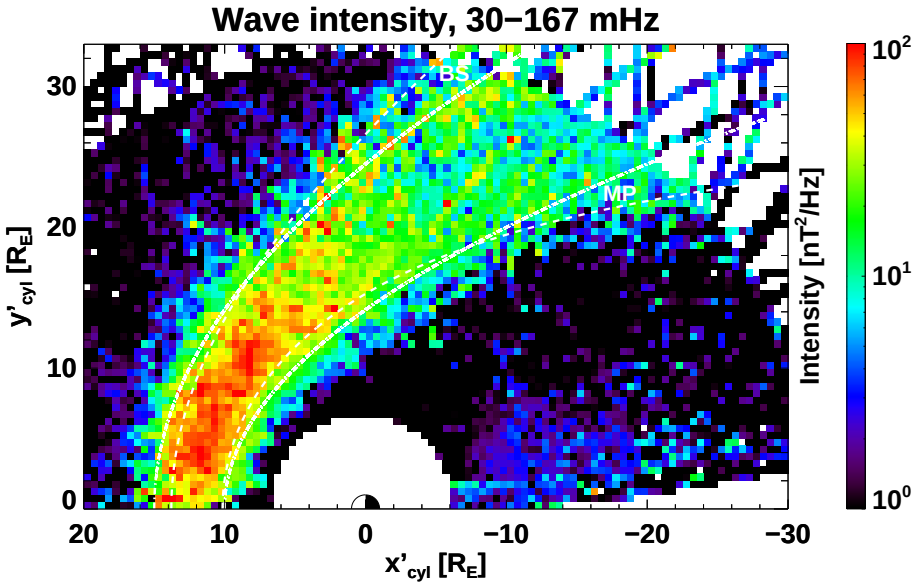

Fig. 2. Spatial distribution of the wave intensity in the frequency range 30 to 167 mHz (after Guicking, 2011). The underlying THEMIS magnetic field data are shown in Fig. 1 as well as the bow shock (BS) and magnetopause (MP) models.

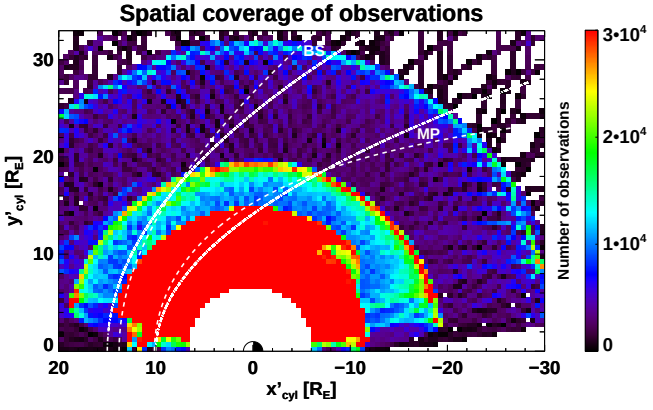

Fig. 3. Spatial coverage of the THEMIS wave intensity observations displayed in Fig. 2 with the same bow shock (BS) and magnetopause (MP) models. The spatial coverage is inhomogeneous due to a better coverage of observations close to Earth. Nonetheless, sufficient observations within a radius of $\sim 30\,R_E$ are available.

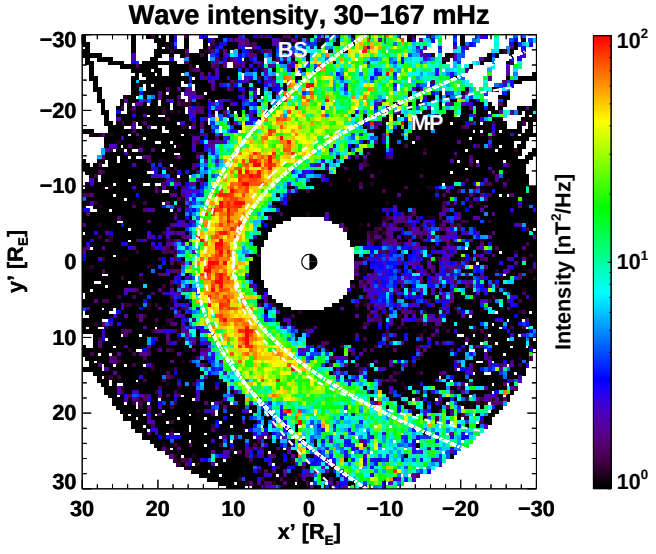

Fig. 4. Spatial distribution of the wave intensity in the ecliptic plane (after Guicking, 2011).

variance directions, respectively. The intensity (wave activity) is then defined as

$$I = \lambda_1 + \lambda_2 - 2\lambda_3, \quad (5)$$

assuming isotropic noise which we consider as a reasonable estimate for our statistical analysis. These intensity values denote a mean spectral density of the chosen frequency band and is at the same time an estimate of the total magnetic energy density over the frequency range. The spatial distribution of the wave intensity I about the mean field is displayed in Fig. 2, with the corresponding spatial coverage of the observations in Fig. 3 (both figures are presented in the same format and have the same bow shock and magnetopause model boundaries as Fig. 1). Since we related the time at the centre of each analysed interval to the spacecraft position, observations are spatially closer to each other during times of lower spacecraft velocity (as e.g. at the apocentre) than during times of higher spacecraft velocity (as e.g. at the pericentre). The calculated intensities are normalised to this spatial coverage of observations (Fig. 3) and thus differences in the observation time are considered.

This analysis procedure has already been applied to the THEMIS data set in Guicking (2011) and the spatial wave intensity distribution (cf. Fig. 2) was presented there. The wave intensity is enhanced in the entire magnetosheath, with peak values in the dayside magnetosheath. Except for the tail region close to the x'_{cyl}-axis where also moderate wave activity can be observed, the wave activity has overall a very low level outside the magnetosheath. Figure 2 shows that the wave intensity decreases with increasing solar zenith angle (SZA; the SZA is the angle between the x'_{cyl}-axis and the line connecting the point of origin with a point on the bow shock), implying that wave energy decays from the bow shock towards downstream regions. The THEMIS orbits are close to the ecliptic plane and thus they provide as well a spatial coverage over all local times for the analysed data set. This is useful for taking into account potential dawn-dusk asymmetries, and Fig. 4 shows (in addition to Fig. 2) the projection of the wave intensity distribution into the ecliptic plane (x'-y'-plane). Figure 4 was also presented in Guicking (2011) and the wave intensity distribution shows no well developed dawn-dusk asymmetry. There is only a slight enhanced wave activity at the dawn side ($-y'$-axis) observable compared to the dusk side ($+y'$-axis), which may be originated from different wave generation processes present in both regions. As we focus in Sect. 4 primarily on the wave intensity evolution in the magnetosheath and not on the identification of wave generation mechanisms and the underlying instabilities, respectively, we will retain the cylindrical coordinate system in the following. Beyond that, the cylindrical coordinates improve the statistical significance of the results as more intensity values per bin are available, but we will also discuss individual results for the dawn region and the dusk region.

Considering that the solar wind plasma is deflected in the magnetosheath around Earth's magnetosphere, we want to study furthermore the wave intensity distribution in connection with the plasma flow, opening also the possibility to compare the results with former studies of the Venusian magnetosheath. Hence, a plasma flow model for Earth's magnetosheath is required and will be introduced in the following section.

3 Magnetosheath streamline model

An analytical streamline model describing the plasma flow in Earth's magnetosheath was adopted from a model by Kobel and Flückiger (1994) developed originally to model the steady state magnetic field in the magnetosheath. The authors comment that the magnetic field lines of their model represent also the streamlines of the solar wind flow around the magnetosphere in case of parallel or antiparallel orientation of the magnetic field direction with respect to the solar wind flow direction upstream of the bow shock. They note that the streamline pattern of their model is for this situation in good qualitative agreement with the streamline pattern of Spreiter and Stahara (1980) determined from numerical calculations. The streamline pattern and velocity distribution derived from the modified Kobel and Flückiger model was already used by e.g. Génot et al. (2011), Tátrallyay et al. (2008), and Tátrallyay and Erdős (2002) to investigate the timing and characterise the evolution of mirror mode structures in the terrestrial magnetoaheath.

Taking as the starting point the Kobel and Flückiger magnetic field model, at first parabolic coordinates (u, v, ϕ) have to be introduced which are related to Cartesian coordinates (x, y, z) via

$$x = uv\cos(\phi), \tag{6}$$

$$y = uv\sin(\phi), \tag{7}$$

$$z = \frac{1}{2}\left(u^2 - v^2\right), \tag{8}$$

with $u \geq 0$, $v \geq 0$, and $0 \leq \phi \leq 2\pi$ (e.g. Madelung, 1957). The parabolic coordinates were also used by Kobel and Flückiger (1994) and e.g. Tátrallyay and Erdős (2005). As our statistical results are presented in a two-dimensional coordinate system (cf. Sect. 2), we reduce the three-dimensional parabolic coordinate system to a two-dimensional representation by setting $\phi = 0$. Models of the bow shock and the magnetopause are determined from the remaining parabolic coordinate equations. The shapes of these two boundaries are intrinsically given by these equations, but the exact stand-off positions are defined by the two parameters (Kobel and Flückiger, 1994)

$$v = v_{BS} = \sqrt{2R_{BS} - R_{MP}}, \tag{9}$$

where R_{BS} is the subsolar stand-off distances of the bow shock and R_{MP} the subsolar stand-off distance of the magnetopause and

$$v = v_{MP} = \sqrt{R_{MP}}. \tag{10}$$

The modelled boundaries thus depend only on their stand-off distances.

Since the origin of the parabolic coordinate system is located halfway between the centre of Earth and the subsolar stand-off distance of the magnetopause and thus shifted from the centre of Earth in opposite direction to the apparent solar wind flow direction, the relation to the cylindrical Cartesian coordinate system introduced in the previous section is given by

$$x'_{cyl} = -z + \frac{1}{2}R_{MP} = -\frac{1}{2}\left(u^2 - v^2\right) + \frac{1}{2}R_{MP} \tag{11}$$

and

$$y'_{cyl} = x = uv. \tag{12}$$

The magnetosheath velocity potential and flow pattern are derived as follows: Adapting the scalar potential of the total magnetic field in the magnetosheath of the Kobel and Flückiger model and substituting the initial magnetic field by the initial solar wind flow velocity yields the velocity potential function (with $\nu_{MP} \leq \nu \leq \nu_{BS}$ and $\phi = 0$)

$$\Phi = -\left(\frac{\nu_{MP}^2 \nu_{BS}^2}{\nu_{BS}^2 - \nu_{MP}^2}\right) v \left(\frac{u^2 - \nu^2}{2\nu_{BS}^2} + \ln(\nu)\right) - v\frac{1}{2}\left(u^2 - \nu^2\right) + C, \quad (13)$$

where each constant Φ represents one velocity potential line, v is the initial flow velocity upstream of the bow shock, and C is an arbitrary constant.

The velocity potential function is defined as the function from which one can derive the velocity in a particular direction by calculating the derivative of the velocity potential function in that direction (e.g. Vallentine, 1967), so the velocity in parabolic coordinates can be defined as (the gradient in parabolic coordinates can be found in e.g. Madelung, 1957)

$$\boldsymbol{v} = -\nabla\Phi = \left(-\lambda\frac{\partial\Phi}{\partial u}, -\lambda\frac{\partial\Phi}{\partial\nu}, -\frac{1}{u\nu}\frac{\partial\Phi}{\partial\phi}\right), \quad (14)$$

where λ is

$$\lambda = \frac{1}{\sqrt{u^2 + \nu^2}}. \quad (15)$$

The two parabolic velocity components v_u and v_ν are then

$$v_u = \left(\frac{\nu_{MP}^2}{\nu_{BS}^2 - \nu_{MP}^2}\right) u v + u v, \quad (16)$$

$$v_\nu = \left(\frac{\nu_{MP}^2}{\nu_{BS}^2 - \nu_{MP}^2}\right)\left(\frac{\nu_{BS}^2}{\nu} - \nu\right) v - \nu v. \quad (17)$$

Streamlines are defined as the lines which are tangential to the velocity vectors (e.g. Vallentine, 1967) and streamlines and velocity potential lines are perpendicular to one another. We can find the streamline function by finding the function Ψ satisfying the equation (the basic idea and a detailed theoretical background of fluid mechanics is presented by e.g. Prandtl et al., 1969)

$$\boldsymbol{v} = -\nabla \times \left[\Psi \boldsymbol{e}_\phi\right], \quad (18)$$

with the ϕ unit vector $\boldsymbol{e}_\phi$ of parabolic coordinates. Equation (18) writes in parabolic coordinates (the expression of the curl in parabolic coordinates is given in e.g. Madelung, 1957) as

$$-\nabla \times \Psi = -\frac{\lambda}{u\nu}\begin{pmatrix} \frac{\partial}{\partial\nu}(u\nu\Psi) \\ -\frac{\partial}{\partial u}(u\nu\Psi) \\ 0 \end{pmatrix} = \begin{pmatrix} v_u \\ v_\nu \\ 0 \end{pmatrix}. \quad (19)$$

The function

$$\Psi = -\left(\frac{\nu_{MP}^2 \nu_{BS}^2}{\nu_{BS}^2 - \nu_{MP}^2}\right) v \left(\frac{u\nu^2 - u\nu_{BS}^2}{2\nu_{BS}^2 \nu}\right) - \frac{u\nu}{2} v \quad (20)$$

satisfies Eq. (18) and Eq. (19), respectively, and is thus the streamline function where each constant Ψ represents a flow line. From Eq. (18) we get with Eq. (20) also the parabolic velocity components (Eq. 16 and Eq. 17).

The only parameters for the parabolic bow shock and magnetopause boundary models are the subsolar stand-off distances. We have chosen the distances $R_{BS} = 15 R_E$ for the bow shock and $R_{MP} = 10 R_E$ for the magnetopause, as then the Slavin and Holzer (1981) and Shue et al. (1997) models overlap qualitatively well with the parabolic boundary model. Choosing a lower bow shock stand-off distance of the parabolic model would lead, especially on the nightside, to diverging bow shock shapes of both models (cf. Figs. 1 to 3).

We discussed the origin of the model in the first paragraph of this chapter and complete the discussion now regarding the validity of the model and the magnitude of the velocity. The Kobel and Flückiger magnetic field line model is valid for arbitrary orientations of the interplanetary magnetic field lines with respect to the solar wind flow direction. Deriving the streamline model from this magnetic field line model assumes geometric equivalence between streamlines (velocity potential lines) and magnetic field lines (potential lines) in case of parallel or antiparallel interplanetary magnetic field line orientation with respect to the upstream solar wind flow direction (cf. Kobel and Flückiger, 1994). Thus, we have an independent static streamline model which is based on a special case of the more general magnetic field line model equations.

In order to calculate the magnitude of the magnetosheath flow velocity v_{MS} based on the original magnetic field model equations, one has to introduce a scaling factor. We use

$$v_{MS} = v_{KF}\left(1 + \frac{\nu_{MP}^2}{\nu_{BS}^2 - \nu_{MP}^2}\right)^{-1}, \quad (21)$$

where v_{KF} is the velocity magnitude obtained by the Kobel and Flückiger model. We have derived the scaling factor empirically on the basis of the resulting velocity contour profile in the magnetosheath. Considering this scaling factor leads for different upstream solar wind velocities to a velocity profile comparable to the magnetosheath velocity profiles obtained by Génot et al. (2011) and Tátrallyay et al. (2008). In particular, we use in our model the same initial solar wind velocity of $|\boldsymbol{v}| = 400\,\mathrm{km/s}$ as Tátrallyay et al. (2008), which is a good estimate for the mean solar wind flow velocity. Génot et al. (2011) and Tátrallyay et al. (2008) state also that their velocity distributions are in good agreement with gasdynamic simulations done by Spreiter and Stahara (1980) and Spreiter et al. (1966). Therefore, we assume the analytical

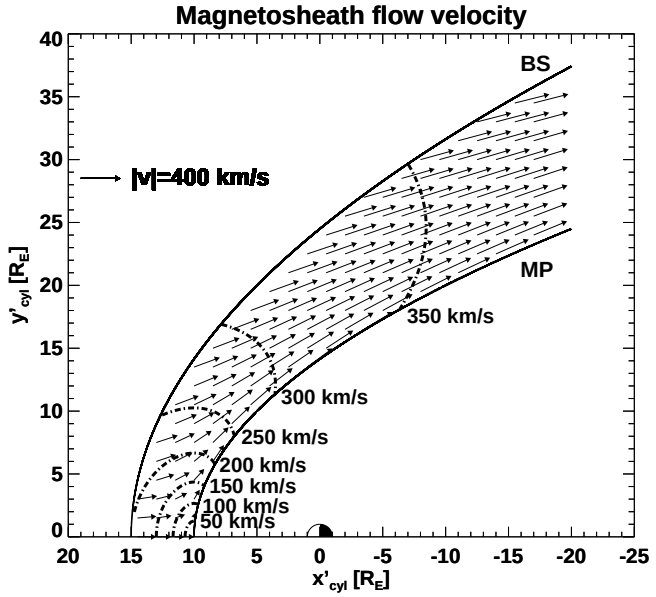

Fig. 5. Flow velocity in Earth's magnetosheath calculated from the analytical streamline model. The dashed-dotted lines mark the velocity contour lines for the listed velocities. The initial solar wind flow velocity in the model is $|\boldsymbol{v}| = 400\,\mathrm{km\,s^{-1}}$. BS and MP denote the bow and the magnetopause models.

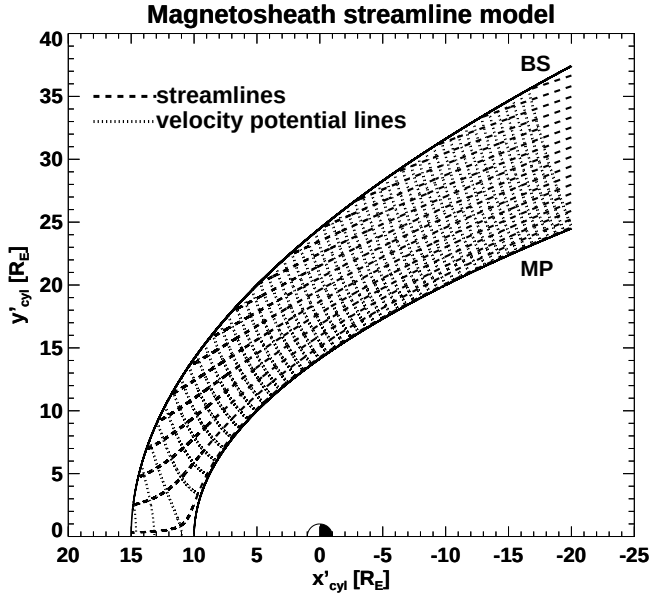

Fig. 6. Streamlines and velocity potential lines of the analytical streamline model in Earth's magnetosheath bounded by the bow shock (BS) and magnetopause (MP) models.

streamline model derived herein to be adequate for our estimate of the wave intensity behaviour in the terrestrial magnetosheath.

The complete model is displayed in cylindrical coordinates in Fig. 5 showing the flow velocity vectors and velocity contour lines, and in Fig. 6 showing the different streamlines and velocity potential lines for Earth's magnetosheath.

Table 1. Decay exponents of the wave intensity in the magnetosheath derived from Fig. 2 (total) as well as for the dawn and dusk side of the magnetosheath derived from Fig. 4.

Number of streamline	decay exponent λ		
	total	dawn	dusk
1	−1.28	−1.66	−1.68
2	−1.23	−1.49	−1.52
3	−1.47	−1.67	−1.56
4	−1.30	−1.55	−1.48
5	−1.46	−1.25	−1.33
6	−1.03	−1.20	−1.28
7	−1.18	−1.86	−1.03
8	−1.07	−1.16	−1.10
9	−0.65	−0.93	−0.54
10	−0.27	−1.18	0.10

4 Evolution of magnetosheath wave intensity

In order to investigate the evolution of wave intensity along particular streamlines, at first a certain number of streamlines and velocity potential lines within the magnetosheath has been calculated from the streamline function (Eq. 20) and the velocity potential function (Eq. 13). Precisely, this was done by choosing a constant difference $\Delta\Psi$ and $\Delta\Phi$ between two neighbouring streamlines and two neighbouring velocity potential lines. The composition of the streamline pattern together with the velocity potential line pattern divides the overall magnetosheath area into multiple smaller subareas (cf. Fig. 6). Each of these polygons is therefore edged by two neighbouring streamlines and two neighbouring velocity potential lines (or the bow shock/magnetopause at the edges of the magnetosheath); we then averaged the intensities over the polygon areas. Thus, it leads finally to the result that a certain number of polygons fills up the magnetosheath with a mean intensity value assigned to each polygon. In this way, the data are binned in another way than before (cf. Fig. 2) considering the situation we want to investigate in this chapter, but ensuring also from the statistical point of view that the choice of $\Delta\Psi$ and $\Delta\Phi$ keeps a sufficient number of intensity values within one polygon.

Then, the streamlines between two streamlines (offset to the streamline below and above is in each case $\Delta\Psi/2$) displayed in Fig. 6 are calculated and the centre of each polygon along the streamlines was determined (cf. Guicking et al., 2010). Figure 7 shows the result of this procedure and Fig. 8 shows the corresponding spatial coverage of observations. It shows that the spatial coverage is better in the dayside magnetosheath and decreases towards the nightside and is mainly caused by the satellite orbits (cf. Fig. 3).

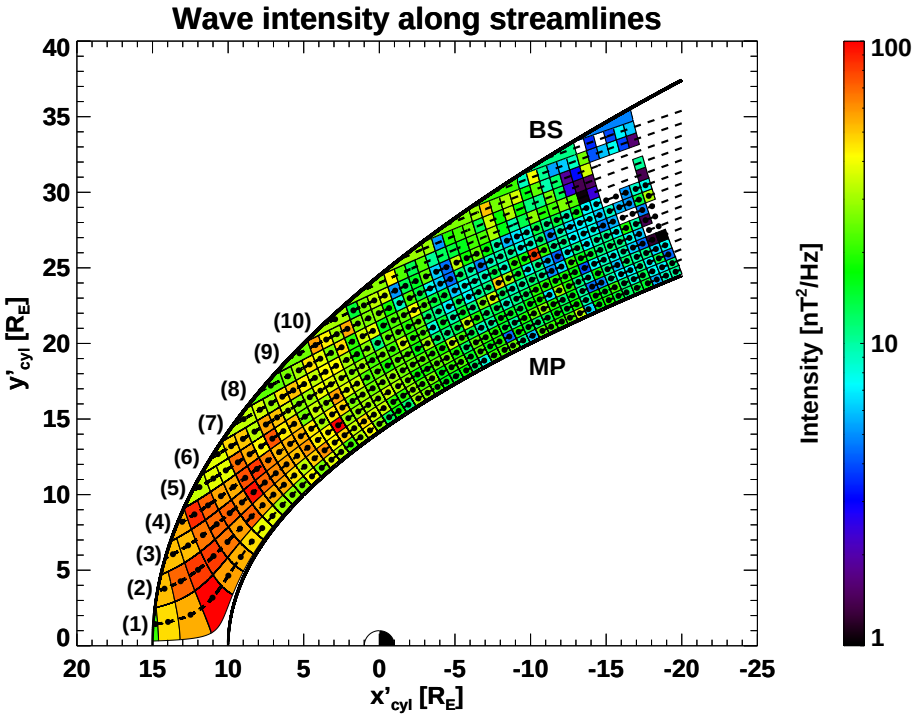

Fig. 7. Evolution of wave intensity along streamlines. The bow shock (BS) and magnetopause (MP) models as well as ten streamlines (dashed lines) which are numbered by (1) to (10) are shown. The spatial and temporal evolution of wave intensity along these ten streamlines is investigated.

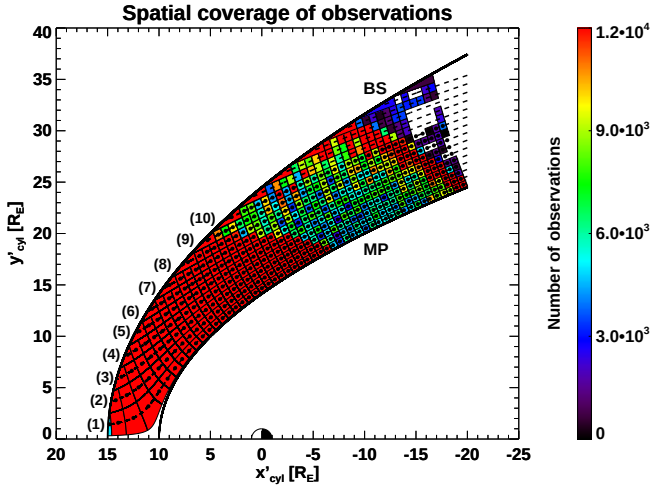

Fig. 8. Spatial coverage of magnetosheath observations displayed in Fig. 7.

Connecting the mean intensities to the coordinates of the polygon centres, we are able to derive an estimate on how the intensity evolves in space and time with the magnetosheath flow. For this purpose, the distance along a streamline starting at the bow shock as well as the elapsed time since the bow shock crossing moving with the flow along a streamline can be calculated. The distance S along a streamline is the line integral along a streamline from the bow shock (BS) to a selected point s_{end} and can be calculated as

$$S = \int_{\mathrm{BS}}^{s_{\mathrm{end}}} \mathrm{d}s, \tag{22}$$

or for the discrete model situation here, the sum over particular distances Δs can be calculated as

$$S = \sum_{k} (\Delta s)_k \,. \tag{23}$$

The elapsed time T since the bow shock crossing is the integral

$$T = \int_{\mathrm{BS}}^{s_{\mathrm{end}}} \frac{1}{v_{\mathrm{MS}}(s)} \mathrm{d}s \tag{24}$$

along a streamline or again in the discrete case

$$T = \sum_{i} \frac{1}{\overline{v}_{\mathrm{MS},i}} (\Delta s)_i \,, \tag{25}$$

where $\overline{v}_{\mathrm{MS},i}$ is the averaged velocity along a distance Δs, so the mean of the velocity at the starting position and at the ending position of each difference Δs. Both parameters, the discrete line element Δs and the mean velocity $\overline{v}_{\mathrm{MS},i}$, are

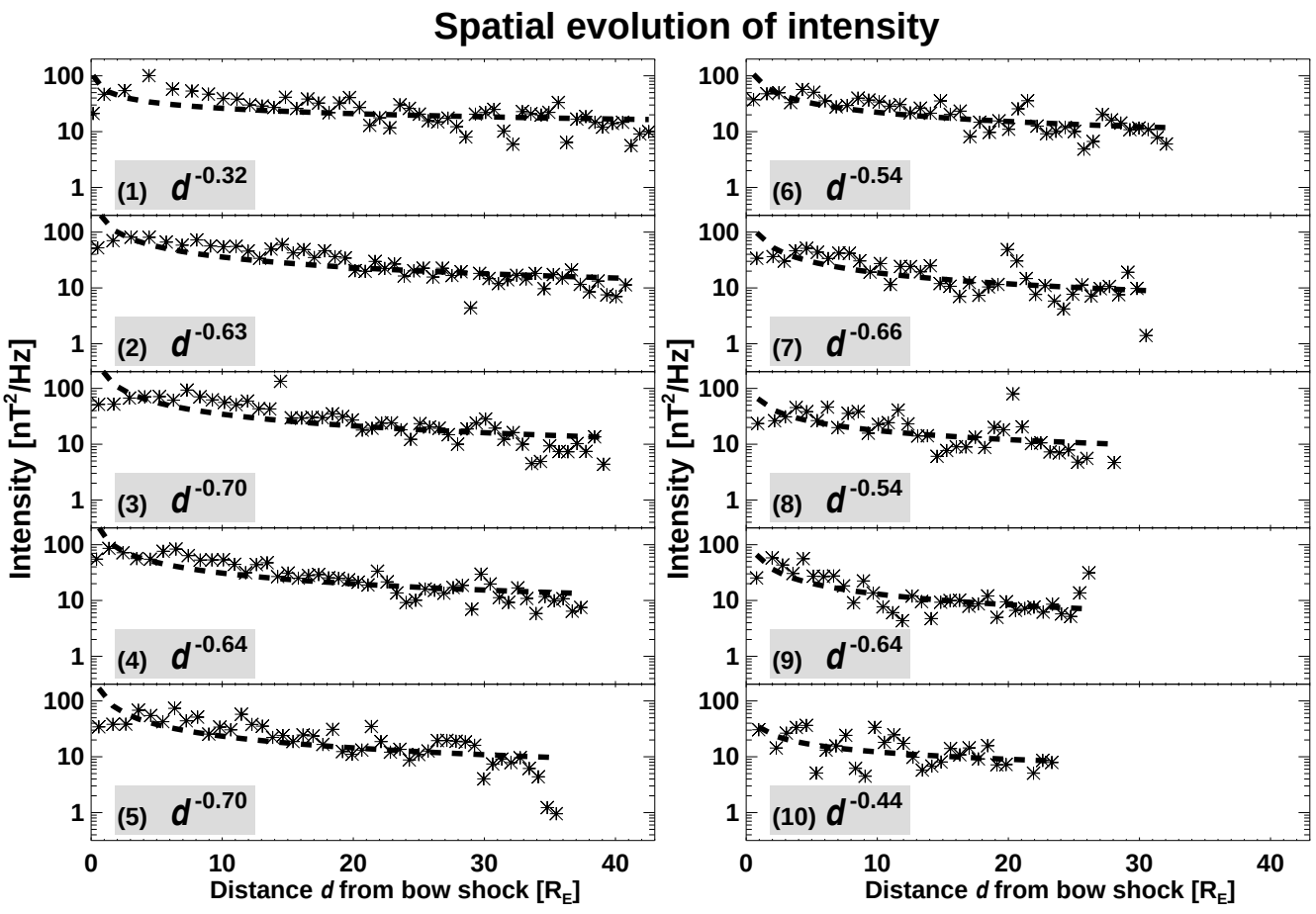

Fig. 9. Wave intensity as function of distance from bow shock. Numbers in parentheses indicate the spatial evolution curve of the associated streamline in Fig. 7. The asterisks denote the calculated intensity values along a streamline and the dashed lines are power law fits to the intensity values. The exponent of the power law represents thus the strength of the decay and varies between -0.32 and -0.70 indicated by d^{β}.

taken from the magnetosheath streamline model introduced in the previous section.

Figure 9 shows the evolution of the wave intensity with distance. Fitting the data with a power law of the form $I = \alpha d^{\beta}$ where I is the intensity and d the distance from the bow shock along a particular streamline confirms quantitatively the visual impression of Fig. 7 where the wave intensity decreases on average with increasing distance. The power law fit reveals exponents β in the range from -0.32 to -0.70. In order to investigate the decay of the fluctuations in terms of turbulent processes in the magnetosheath and especially in terms of a theoretical decay model as well as in order to compare our study with the results for Venus, we have to derive furthermore the temporal evolution of the wave intensity.

The basic theoretical model we compare and discuss our results with is the theoretical concept of freely evolving/decaying turbulence. It describes the behaviour of a turbulent flow when there was once energy injected into the system and the system is then left to its own resources. In particular, this turbulence model describes the dissipation of the fluctuating part of the energy while the fluctuations are convected with the flow. The magnetic energy density E of the fluctuations, which is equivalent to the wave intensity I we calculated[1], follows then the power law

$$E \propto t^{\lambda} \tag{26}$$

with $\lambda = -10/7 \approx 1.43$ as a result of the hydrodynamic turbulence model by Kolmogorov (1941), and $\lambda = -2/3$ for the magnetohydrodynamic case (Biskamp, 2003). Figure 10 shows the evolution of wave intensity with time. We fitted a power law of the form $I = \gamma t^{\lambda}$, where I is again the intensity and t the elapsed time since the bow shock crossing along a particular streamline to the decaying part of the intensities and one reveals exponents λ which lie in the range from -0.27 to -1.47. In addition, we determined the exponents

[1] $E = C\,I$ where C is a constant comprised of the number of frequency samples and the frequency resolution of the power spectra (cf. Guicking et al., 2010)

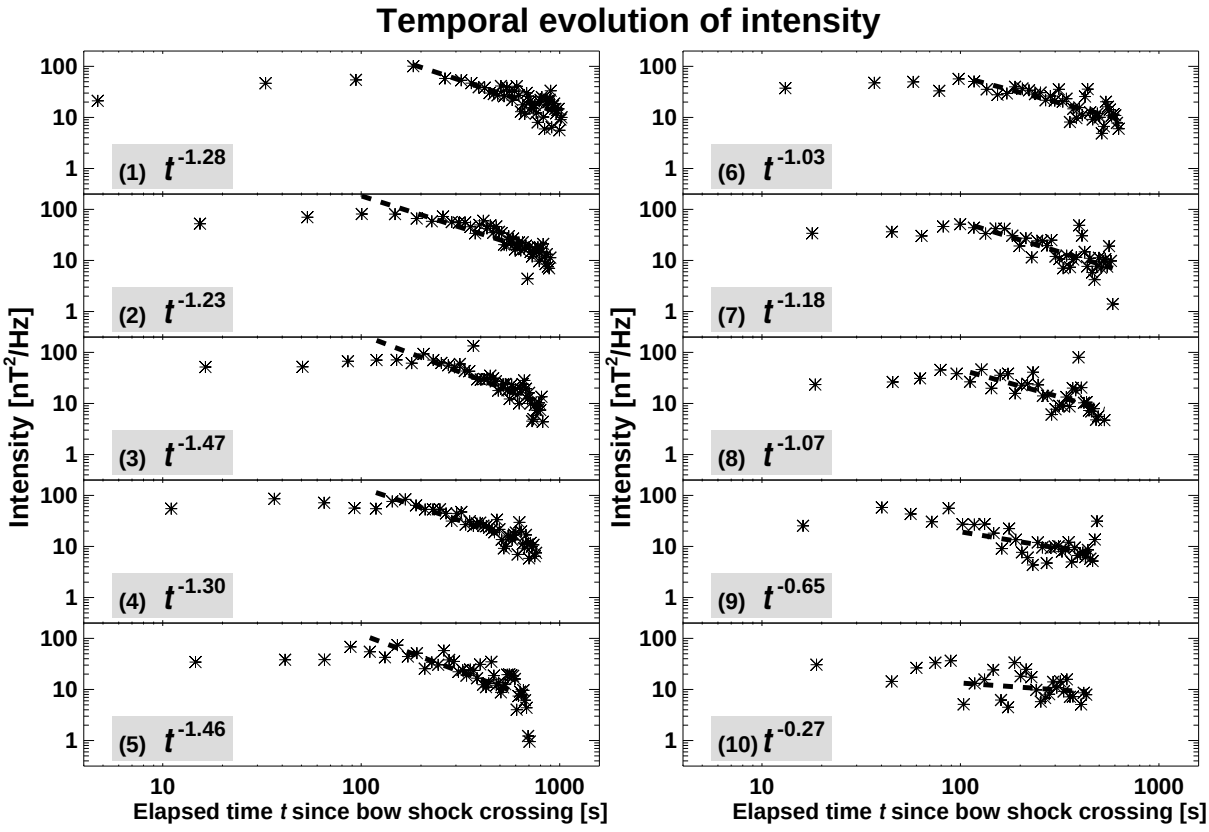

Fig. 10. Wave intensity as function of the elapsed time since bow shock crossing. Numbers in parentheses indicate the evolution curve of the associated streamline in Fig. 7. The asterisks denote the calculated intensity values along a streamline and the dashed lines are straight lines in the double-logarithmic plots which were fitted to the intensities. The straight lines' slope is in non-logarithmic scale the exponent of a power law and represents thus the strength of the decay. The decay along a particular streamline is indicated by t^{λ} where λ varies between -0.27 and -1.47.

separately for the dawn side and the dusk side on the basis of the wave intensity distribution presented in Fig. 4. In Table 1 the results are listed.

As the exact solution of Eq. (26) is

$$E = E_0 \, (t - t_0)^{-\lambda} \,, \tag{27}$$

where t_0 is the initial eddy-turnover time, the power law behaviour becomes clearly visible for $t \gg t_0$ (Biskamp, 2003). For this reason, intensity values close to the bow shock with an elapsed time below 100 s are neglected for the power law fit and only the decaying party is approximately considered. Accompanied by this choice we can give also an estimate of t_0, which is about tens of seconds up to about 100 s.

Plotting the wave intensity as the function of the elapsed time assumes Taylor's hypothesis, meaning that the velocity of the fluctuations, e.g. the phase velocity of a wave, is much smaller than the mean flow velocity. The validity of this assumption will be discussed in more detail in the final section.

5 Discussion and conclusions

The observed low-frequency wave activity in Earth's plasma environment in the range 30 to 167 mHz (cf. Fig. 2) concentrates almost entirely on the magnetosheath, and thus one can expect a connection with plasma physical processes at the bow shock and its vicinity as well as inside the magnetosheath which provide sources of wave energy. The first data points in each panel in Fig. 10 (below 100 s) which do not belong to the decaying part of the plotted data points could represent the area where instabilities rise and wave generation processes are dominant, respectively, and thus energy is injected. Later (above 100 s), a turbulent energy cascade begins, characterised by an energy decay following in good approximation a power law. We therefore conclude that instabilities and wave generation processes can be referred rather to the bow shock and its vicinity, and a developed turbulent state rather to the deeper magnetosheath away from the bow shock. Since the magnetopause prevents efficiently the penetration of solar wind particles into the magnetosphere, as a result the solar wind is deflected around the magnetosphere and the spatial distribution of magnetosheath wave activity

may be coupled with properties of the magnetosheath flow pattern.

The observed spatial and temporal decay of magnetosheath wave intensity along streamlines leads us to the interpretation that the bow shock may play a substantial role in this process. Our observations in the terrestrial magnetosheath are in good qualitative and quantitative agreement with theoretical considerations of freely evolving/decaying turbulence since they reveal a wave energy decay with decay exponents λ (cf. Sect. 4) in the approximate range of hydrodynamic ($\lambda = -10/7$) and magnetohydrodynamic ($\lambda = -2/3$).

The mean of the first five exponents (streamlines 1 to 5 which pass through the lower magnetosheath) is $\lambda_{\text{mean,1-5}} = -1.35$ with a standard deviation of $\sigma_{1\text{-}5} = 0.11$, and the mean of the following five exponents (streamlines 6 to 10 which pass through the upper magnetosheath) is $\lambda_{\text{mean,6-10}} = -0.84$ with a standard deviation of $\sigma_{6\text{-}10} = 0.38$. Hence, the energy decay in the lower magnetosheath is on average steeper than in the upper magnetosheath, and we can interpret that in the upper magnetosheath more sources of energy may be present than in the lower magnetosheath. However, the exponent of the first streamline ($\lambda_1 = -1.28$) which passes the magnetosheath closest to the magnetopause is close to the mean exponent ($\lambda_{\text{mean,1–5}} = -1.35$), and thus no unique behaviour characterises the wave intensity evolution at the magnetopause compared to the rest of the lower magnetosheath.

Furthermore, we determined the decay exponents λ for the dawn region and the dusk region (cf. Table 1). The means of the lower magnetosheath are $\lambda_{\text{mean,dawn,1–5}} = -1.52$ ($\sigma_{\text{dawn,1–5}} = 0.17$) and $\lambda_{\text{mean,dusk,1–5}} = -1.51$ ($\sigma_{\text{dusk,1–5}} = 0.13$), and the means of the upper magnetosheath are $\lambda_{\text{mean,dawn,6–10}} = -1.27$ ($\sigma_{\text{dawn,6–10}} = 0.35$) and $\lambda_{\text{mean,dusk,6–10}} = -0.77$ ($\sigma_{\text{dusk,6–10}} = 0.56$). In the lower magnetosheath the projection to the ecliptic plane reveals decay exponents which yield a slightly steeper decay than predicted for hydrodynamic turbulence, but no dawn-dusk asymmetry can be observed. In the upper magnetosheath the dawn side shows a slightly steeper decay than the dusk side, but one has to note that the standard deviation is higher than in the lower magnetosheath. We conclude from these observations that dawn-dusk dependent wave generation mechanisms and instabilities, respectively, may influence the evolution of the wave intensity only in the upper magnetosheath. On average, increasing and differing (in case of the dawn-dusk distinction) exponents with increasing streamline numbers may also be partly caused by a reduced number of data points due to limitations in the spatial coverage of observations.

One has to note that the wave intensity as a function of time assumes Taylor's hypothesis, which means that the phase velocity of waves in the plasma frame of reference should be much smaller than the plasma flow velocity. Hence, this assumption is well justified for e.g. mirror modes which have a zero phase velocity, slowly propagating waves with regard to the plasma flow velocity and downstream propagating waves. Upstream propagating waves with velocities comparable to the plasma flow velocity would increase the time scale and Taylor's hypothesis may become inappropriate. At this point, we accept such limitations of our model as we do not distinguish between different wave modes, but want to get a quantitative estimate of the observed wave intensity decay in the magnetosheath which is the result of the statistically analysed THEMIS magnetic field data set.

As already suggested by several authors (e.g. Génot et al., 2011; Tátrallyay et al., 2008; Tátrallyay and Erdős, 2005, 2002; Schwartz et al., 1996; Gary et al., 1993; Gary, 1993, 1991), different wave energy sources and wave generation mechanisms exciting low-frequency wave modes are believed to be present in Earth's magnetosheath. Sources are mainly processes upstream of or at the bow shock and processes within the magnetosheath; the presence of Alfvén/ion-cyclotron and mirror modes are often discussed in this context. However, individual modes are favoured by parameters like e.g. the plasma-β or the configuration like e.g. the bow shock geometry.

In this study, we are able to compare the derived wave activity with observations in the Venusian plasma environment as the analysis of the magnetic field data was done in a similar way. Guicking et al. (2010) determined the spatial distribution of low-frequency magnetic field fluctuations at Venus in the frequency range 30 to 300 mHz. Although both frequency ranges, the frequency range discussed here in the case of Earth and the frequency range discussed in the case of Venus, do not overlap exactly and vary with respect to the proton gyrofrequency, respectively, a qualitative comparison is justified because both ranges reflect the low-frequency range for the most part. Comparing Fig. 2 with the results of Guicking et al. (2010) for Venus, we observe a qualitative difference between both observations: while at Venus the wave activity decreases from the subsolar magnetosheath region towards the terminator rapidly, at Earth a significant amount of wave intensity is also present on the nightside (the dayside magnetosheaths of both planets contain each the highest wave activities compared to the other regions).

As fluctuations in the magnetosheath are often considered to be in a turbulent state, the transport of wave energy related to turbulence was discussed. At Venus the turbulent character of magnetic field fluctuations was suggested by Winske (1986) and Luhmann et al. (1983), and Guicking et al. (2010) report on a qualitative agreement between their observations and the concept of freely evolving/decaying turbulence (e.g. Davidson, 2004; Biskamp, 2003), assuming that waves are mainly generated at the bow shock and convected downstream with the plasma flow. For the Venusian magnetosheath they found exponents λ (cf. Sect. 4) from -1.7 to -3.9.

The above mentioned qualitatively differing intensity distribution at Earth compared to Venus is also reflected by the quantitative results concerning the temporal decay of

wave intensity along magnetosheath streamlines. At Earth the decay is flatter than at Venus and for this reason it matches better with the theoretical predictions of freely evolving/decaying turbulence, meaning that the exponents λ are closer to the values for hydrodynamic and magnetohydrodynamic turbulence. Hence, the results are consistent with the scenario that the wave energy decays due to a turbulent cascade while waves are convected downstream with the plasma flow and imply that wave generation for the selected frequency range occurs mainly in the vicinity of the bow shock.

The different type of interaction process between the solar wind and the planetary obstacles influences and characterises the wave activity distributions, since Earth compared to Venus is surrounded by its own intrinsic magnetic field, causing a different size and configuration of the magnetosheath and may favour different or additional plasma physical processes.

The aim of this investigation is to present the global statistical wave activity distribution based on a comprehensive THEMIS magnetometer data set which provides a large spatial coverage of the terrestrial plasma environment and to provide a theoretical interpretation of the observations.

Acknowledgements. This work was financially supported by the German Ministerium für Wirtschaft und Technologie and the Deutsches Zentrum für Luft- und Raumfahrt under grant 50OC1001 and by the Deutsche Forschungsgemeinschaft under grant MO 539/17-1. The authors want to thank Daniel Heyner for fruitful discussions.

Topical Editor I. A. Daglis thanks J. De Keyser and one anonymous referee for their help in evaluating this paper.

References

Anderson, B. J., Fuselier, S. A., Gary, S. P., and Denton, R. E.: Magnetic spectral signatures in the Earth's magnetosheath and plasma depletion layer, J. Geophys. Res., 99, 5877–5891, doi:10.1029/93JA02827, 1994.

Angelopoulos, V.: The THEMIS Mission, Space Sci. Rev., 141, 5–34, doi:10.1007/s11214-008-9336-1, 2008.

Angelopoulos, V.: The ARTEMIS Mission, Space Sci. Rev., 165, 3–25, doi:10.1007/s11214-010-9687-2, 2011.

Auster, H.-U., Glassmeier, K.-H., Magnes, W., Aydogar, O., Baumjohann, W., Constantinescu, D., Fischer, D., Fornaçon, K.-H., Georgescu, E., Harvey, P., Hillenmaier, O., Kroth, R., Ludlam, M., Narita, Y., Nakamura, R., Okrafka, K., Plaschke, F., Richter, I., Schwarzl, H., Stoll, B., Valavanoglou, A., and Wiedemann, M.: The THEMIS Fluxgate Magnetometer, Space Sci. Rev., 141, 235–264, doi:10.1007/s11214-008-9365-9, 2008.

Biskamp, D.: Magnetohydrodynamic Turbulence, Cambridge Univ. Press, Cambridge, 2003.

Davidson, P. A.: Turbulence: An introduction for scientists and engineers, Oxford Univ. Press, New York, 2004.

Denton, R. E., Lessard, M. R., LaBelle, J. W., and Gary, S. P.: Identification of low-frequency magnetosheath waves, J. Geophys. Res., 103, 23661–23676, doi:10.1029/98JA02196, 1998.

Du, J., Zhang, T. L., Baumjohann, W., Wang, C., Volwerk, M., Vörös, Z., and Guicking, L.: Statistical study of low-frequency magnetic field fluctuations near Venus under the different interplanetary magnetic field orientations, J. Geophys. Res., 115, A12251, doi:10.1029/2010JA015549, 2010.

Escoubet, C. P., Fehringer, M., and Goldstein, M.: Introduction: The Cluster mission, Ann. Geophys., 19, 1197–1200, doi:10.5194/angeo-19-1197-2001, 2001.

Espley, J. R., Cloutier, P. A., Brain, D. A., Crider, D. H., and Acuña, M. H.: Observations of low-frequency magnetic oscillations in the Martian magnetosheath, magnetic pileup region, and tail, J. Geophys. Res., 109, A07213, doi:10.1029/2003JA010193, 2004.

Frey, S., Angelopoulos, V., Bester, M., Bonnell, J., Phan, T., and Rummel, D.: Orbit Design for the THEMIS Mission, Space Sci. Rev., 141, 61–89, doi:10.1007/s11214-008-9441-1, 2008.

Gary, S. P.: Electromagnetic ion/ion instabilities and their consequences in space plasmas: A review, Space Sci. Rev., 56, 373–415, doi:10.1007/BF00196632, 1991.

Gary, S. P.: Theory of Space Plasma Microinstabilities, Cambridge atmospheric and space science series, Cambridge Univ. Press, New York, 1993.

Gary, S. P., Fuselier, S. A., and Anderson, B. J.: Ion anisotropy instabilities in the magnetosheath, J. Geophys. Res., 98, 1481–1488, doi:10.1029/92JA01844, 1993.

Génot, V., Broussillou, L., Budnik, E., Hellinger, P., Trávníček, P. M., Lucek, E., and Dandouras, I.: Timing mirror structures observed by Cluster with a magnetosheath flow model, Ann. Geophys., 29, 1849–1860, doi:10.5194/angeo-29-1849-2011, 2011.

Guicking, L.: Niederfrequente Magnetfeldfluktuationen in der Plasmaumgebung der Venus, Ph.D. thesis, Technische Universität Braunschweig, 2011.

Guicking, L., Glassmeier, K.-H., Auster, H.-U., Delva, M., Motschmann, U., Narita, Y., and Zhang, T. L.: Low-frequency magnetic field fluctuations in Venus' solar wind interaction region: Venus Express observations, Ann. Geophys., 28, 951–967, doi:10.5194/angeo-28-951-2010, 2010.

Kobel, E. and Flückiger, E. O.: A model of the steady state magnetic field in the magnetosheath, J. Geophys. Res., 99, 23617–23622, doi:10.1029/94JA01778, 1994.

Kolmogorov, A. N.: The Local Structure of Turbulence in Incompressible Viscous Fluid for Very Large Reynolds Numbers, Dokl. Akad. Nauk SSSR, 30, 301–305, (reprinted in P. Roy. Soc. A, 434, 9–13, 1991), 1941.

Liu, W., Sarris, T. E., Li, X., Elkington, S. R., Ergun, R., Angelopoulos, V., Bonnell, J., and Glassmeier, K. H.: Electric and magnetic field observations of Pc4 and Pc5 pulsations in the inner magnetosphere: A statistical study, J. Geophys. Res., 114, A12206, doi:10.1029/2009JA014243, 2009.

Liu, W., Sarris, T. E., Li, X., Ergun, R., Angelopoulos, V., Bonnell, J., and Glassmeier, K. H.: Solar wind influence on Pc4 and Pc5 ULF wave activity in the inner magnetosphere, J. Geophys. Res., 115, A12201, doi:10.1029/2010JA015299, 2010.

Luhmann, J. G., Tátrallyay, M., Russell, C. T., and Winterhalter, D.: Magnetic field fluctuations in the Venus magnetosheath, Geophys. Res. Lett., 10, 655–658, doi:10.1029/GL010i008p00655, 1983.

Madelung, E.: Die mathematischen Hilfsmittel des Physikers, Die Grundlehren der mathematischen Wissenschaften – Band 4, Springer, Berlin, Göttingen, Heidelberg, 6th edn., 1957.

Narita, Y. and Glassmeier, K.-H.: Dispersion analysis of low-frequency waves through the terrestrial bow shock, J. Geophys. Res., 110, A12215, doi:10.1029/2005JA011256, 2005.

Narita, Y. and Glassmeier, K.-H.: Propagation pattern of low frequency waves in the terrestrial magnetosheath, Ann. Geophys., 24, 2441–2444, doi:10.5194/angeo-24-2441-2006, 2006.

Plaschke, F., Glassmeier, K.-H., Sibeck, D. G., Auster, H. U., Constantinescu, O. D., Angelopoulos, V., and Magnes, W.: Magnetopause surface oscillation frequencies at different solar wind conditions, Ann. Geophys., 27, 4521–4532, doi:10.5194/angeo-27-4521-2009, 2009.

Prandtl, L., Oswatitsch, K., and Wieghardt, K.: Strömungslehre, Vieweg, Braunschweig, 7th edn., 1969.

Schäfer, S., Glassmeier, K.-H., Narita, Y., Fornaçon, K. H., Dandouras, I., and Fränz, M.: Statistical phase propagation and dispersion analysis of low frequency waves in the magnetosheath, Ann. Geophys., 23, 3339–3349, doi:10.5194/angeo-23-3339-2005, 2005.

Schwartz, S. J., Burgess, D., and Moses, J. J.: Low-frequency waves in the Earth's magnetosheath: present status, Ann. Geophys., 14, 1134–1150, doi:10.1007/s00585-996-1134-z, 1996.

Shue, J., Chao, J. K., Fu, H. C., Russell, C. T., Song, P., Khurana, K. K., and Singer, H. J.: A new functional form to study the solar wind control of the magnetopause size and shape, J. Geophys. Res., 102, 9497–9511, doi:10.1029/97JA00196, 1997.

Sibeck, D. G. and Angelopoulos, V.: THEMIS Science Objectives and Mission Phases, Space Sci. Rev., 141, 35–59, doi:10.1007/s11214-008-9393-5, 2008.

Slavin, J. A. and Holzer, R. E.: Solar wind flow about the terrestrial planets – 1. Modeling bow shock position and shape, J. Geophys. Res., 86, 11401–11418, doi:10.1029/JA086iA13p11401, 1981.

Song, P. and Russell, C. T.: Time Series Data Analyses in Space Physics, Space Sci. Rev., 87, 387–463, doi:10.1023/A:1005035800454, 1999.

Spreiter, J. R. and Stahara, S. S.: A new predictive model for determining solar wind-terrestrial planet interactions, J. Geophys. Res., 85, 6769–6777, doi:10.1029/JA085iA12p06769, 1980.

Spreiter, J. R., Summers, A. L., and Alksne, A. Y.: Hydromagnetic flow around the magnetosphere, Planet. Space Sci., 14, 223–253, doi:10.1016/0032-0633(66)90124-3, 1966.

Tátrallyay, M. and Erdős, G.: The evolution of mirror mode fluctuations in the terrestrial magnetosheath, Planet. Space Sci., 50, 593–599, doi:10.1016/S0032-0633(02)00038-7, 2002.

Tátrallyay, M. and Erdős, G.: Statistical investigation of mirror type magnetic field depressions observed by ISEE-1, Planet. Space Sci., 53, 33–40, doi:10.1016/j.pss.2004.09.026, 2005.

Tátrallyay, M., Erdős, G., Balogh, A., and Dandouras, I.: The evolution of mirror type magnetic fluctuations in the magnetosheath based on multipoint observations, Adv. Space Res., 41, 1537–1544, doi:10.1016/j.asr.2007.03.039, 2008.

Vallentine, H. R.: Applied hydrodynamics, Butterworths, London, 2nd edn., 1967.

Winske, D.: Origin of large magnetic fluctuations in the magnetosheath of Venus, J. Geophys. Res., 91, 11951–11957, doi:10.1029/JA091iA11p11951, 1986.